

Camelid Heavy-Chain Variable Domains Provide Efficient Combining Sites to Haptens[†]

Silvia Spinelli,[‡] Leon G. J. Frenken,[§] Pim Hermans,[§] Theo Verrips,[§] Kieron Brown,[‡] Mariella Tegoni,[‡] and Christian Cambillau^{*,‡}

Architecture et Fonction des Macromolécules Biologiques, CNRS, UPR-9039, 31 Chemin Joseph Aiguier, 13402 Marseille Cedex 20, France, and Unilever Research Laboratory, Olivier van Noortlaan 120, 3133 AT Vlaardingen, The Netherlands

Received August 5, 1999; Revised Manuscript Received November 17, 1999

ABSTRACT: Camelids can produce antibodies devoid of light chains and CH1 domains (Hamers-Casterman, C. et al. (1993) *Nature* 363, 446–448). Camelid heavy-chain variable domains (VHH) have high affinities for protein antigens and the structures of two of these complexes have been determined (Desmyter, A. et al. (1996) *Nature Struct. Biol.* 3, 803–811; Decanniere, K. et al. (1999) *Structure* 7, 361–370). However, the small size of these VHHs and their monomeric nature bring into question their capacity to bind haptens. Here, we have successfully raised llama antibodies against the hapten azo-dye Reactive Red (RR6) and determined the crystal structure of the complex between a dimer of this hapten and a VHH fragment. The surface of interaction between the VHH and the dimeric hapten is large, with an area of ca. 300 Å²; this correlates well with the low-dissociation constant of 22 nM measured for the monomer. The VHH fragment provides an efficient combining site to the RR6, using its three CDR loops. In particular, CDR1 provides a strong interaction to the hapten through two histidine residues bound to its copper atoms. VHH fragments might, therefore, prove to be valuable tools for selecting, removing, or capturing haptens. They are likely to play a role in biotechnology extending beyond protein recognition alone.

Since the discovery of camelid antibodies devoid of light chains and CH1 domains (1), their heavy-chain variable domains (VHH) have been proposed as valuable potential tools for biotechnology (2, 3). The size of these VHH fragments is reduced to a bare minimum (a single immunoglobulin domain) and their levels of expression and solubility are significantly higher than those of classical Fab or Fvs (2, 3). Several VHHs have been raised against different bacterial or protein antigens (2–4). Three X-ray structures of such VHHs are presently available; two are of camel VHHs in complex with lysozyme (Lys–VHH) (5) and with RNase A (RNase–VHH) (6), respectively, the other is of a llama unliganded anti-hCG VHH (hCG–VHH) (7). VHHs from llama or camel have affinity constants for their protein antigens that are comparable to those of Fab or Fvs (2–4, 8, 9). The VH–antigen interface may display peculiar features such as in the Lys–VHH structure where the very long CDR3 fills the active site, mimicking a saccharide ligand (5, 8). In the case of the hCG–VHH, the absence of bound antigen makes it difficult to draw definitive conclusions, although the shape of the interface and the much shorter CDR3 suggest a more classical combining interface (7). In the case of antibodies containing both heavy and light chains, binding of small hydrophobic antigens usually occurs

deep in the hydrophobic cleft at the VL–VH interface and thus involves framework residues (10, 11). It is expected that the combining site of the VHH is unable to generate a VL–VH-like crevice. Camelid VHHs have been found to be difficult to raise against haptens (LF, unpublished data). Recently, however, several antibodies have been raised against BSA-coupled synthetic haptens in llamas. We report here the first example of a VHH from llama complexed with the copper containing dye, RR6, and demonstrate that camelid VHHs can provide cavities to accommodate haptens, even in the absence of a VL.

MATERIAL AND METHODS

VHH Preparation and Characterization. A male llama (*Lama glama*) was immunized with a BSA (Sigma, A7888) coupled RR6 azo-dye (ICI, Procion Rubine MX-B). Young adult male llamas were injected at days 0, 21, and 35 with 250 mg of the antigens mentioned above in specol (ID-DLO, Lelystad, The Netherlands). Blood samples of about 150 mL were taken seven days after the last immunization and peripheral blood cells were obtained via Ficoll (Pharmacia) discontinuous gradient centrifugation. From these cells, total RNA was isolated and synthesis of the first strand c-DNA was performed (Amersham first strand cDNA kit). DNA fragments encoding VHH domain were amplified by PCR using specific primers and were ligated into a *Saccharomyces cerevisiae* expression plasmid. After transformation of *S. cerevisiae*, the culture supernatants of single colonies were tested via ELISA for the production of RR6-specific VHH fragments. Several VHHs were obtained at very high yields

[†] This work was supported by the EU BIOTECH Structural Biology project (BIO4 CT98-048).

[‡] CNRS, UPR-9039.

[§] Unilever Research Laboratory.

* Corresponding author. Telephone: 33-4-91-16-45-01. Fax: 33-491-16-45-36. E-mail: cambillau@afmb.cnrs-mrs.fr.

(up to 100 mg/L of flask culture). The R2 anti-RR6 fragment was purified from crude yeast culture broth by affinity chromatography, using a Protein-A Sepharose FF column (Pharmacia). More details of the VHH production procedure have been published elsewhere (12). Kinetic measurements were performed using a IAsys Biosensor Instrument (Fisons) in PBS (10 mM Na₂HPO₄, 1 mM KH₂PO₄, 137 mM NaCl, pH 7.4) with 0.05% (v/v) Tween-20, pH 7.4. RR6 was linked to amino silane cuvettes. At least 10 dilutions were injected into the cuvette. The resulting data were analyzed using the FASTFIT software considering the association phase resulting in association and dissociation constants. The values for the R2 VHH fragments were $k_{\text{on}} = 1.5 \times 10^5 \text{ M}^{-1} \text{ s}^{-1}$, $k_{\text{off}} = 3.3 \times 10^{-3} \text{ s}^{-1}$, and $K_d = 22 \text{ nM}$ (12, since these values have been obtained with a biosensor chip, they might be in error by a factor up to 10 and should, therefore, be compared only with values obtained using the same technique).

Crystallization and Data Collection. Red prismatic crystals were obtained after one month using the hanging-drop vapor diffusion method at 20 °C. Drops consisting of 2 μL of a protein solution with the hapten (hapten 5 mM and VHH 11 mg/mL in 10 mM Tris, pH 7.5) were mixed with 2 μL of the wells solution (1.3 M ammonium sulfate, 100 mM sodium acetate, pH 4.2, and 6–7% glycerol). Crystals belong to the space group $P3_221$ with cell dimensions $a = b = 46.7 \text{ \AA}$, $c = 121.1 \text{ \AA}$. The diffraction data were collected on BM14 at the ESRF (Grenoble, France) where the wavelength was chosen in order to optimize the anomalous absorption of the copper ion present in the hapten. Data were indexed using DENZO (13) and merged/scaled using SCALA (14). An anomalous difference Patterson was calculated to localize the copper ions and was interpreted by the program SHELXS (15). Two copper atoms were found to be present for one VHH fragment.

X-ray Structure Solution. Both rotational and translational searches for RR6–VHH were performed with the program AMoRe (16) using the Lys–VHH as the search model (5). The orientation of the variable domain was given by the first highest peak in the corresponding rotation functions calculated with data between 6.0 and 2.8 \AA . The resulting model gave an R -factor of 0.41 and a correlation coefficient of 0.59. All maps were calculated using the CCP4 suite of programs (14). These maps were inspected by the graphics program Turbo-Frodo (17). The model was improved by iterative manual building and refinement using data between 12.0 and 2.5 \AA ; the refinement involved low-resolution bulk solvent correction, positional, B -factor and phase annealing techniques (18) as implemented in the program XPLOR version 3.843 (19). The results of the data reduction and of the refinement are presented in Table 1. The coordinates of the VHH–RR6 complex have been deposited in the Protein Data Bank (<http://www.rcsb.org/pdb/>; accession number 1QD0).

RESULTS AND DISCUSSION

The VHH–RR6 Crystal Structure. The anti-RR6–VHH fragment is a 117 residue monomer of 11 kDa with the classical immunoglobulin fold. It has a high-sequence homology to the other two VHH fragments whose structures are presently known (Figure 1). The RR6 hapten is an azo-dye composed of three groups (Figure 2a): the *p*-sulfonic-phenol moiety (P), the di-sulfonic-naphthol moiety (N), and

Table 1: Data Collection, Structure Determination, and Refinement Summary

data collection	
total/unique number of reflections	57 351/8364
% of data with $I/s I > 1$ (overall/last shell) ^a	96/85
% of data with $I/s I > 3$ (overall/last shell) ^a	88/62
R -merge (%) (overall/last shell) ^a	6/25
refinement	
number of protein/solvent atoms	1053/54
number of reflections (12.0–2.5 \AA)	8157
R -/ R -free value (%) (12.0–2.5 \AA)	21/28
r.m.s.d. on bonds (\AA) & angles (deg)	0.016/1.3
r.m.s.d. on impropers and dihedral (deg)	1.03/27
mean B -factor (\AA^2): main-chain atoms	24.6
side-chain atoms/solvent	24.7/31.1
haptens all atoms, parts 1 & 2 ^b	21.5/12.3/41

^a Overall data: 30.0–2.5 \AA ; last shell: 2.6–2.5 \AA . ^b Part 1 corresponds to the P1 + N1 groups imbedded in the VHH crevice. Part 2 corresponds to the rest of the molecule and comprises the T, N2 and P2 groups.

the triazine reactive ring (T). The two hydroxyl (or hydroxylate) groups and a nitrogen atom of the azo group provide the internal ligation of the copper ion. The dissociation constant between the anti-RR6–VHH and its hapten, determined using a biosensor, is 22 nM. After obtaining crystals whose red color indicated the presence of RR6, the structure was solved by molecular replacement using the Lys–VHH model (5) and has been refined to 2.5 \AA resolution (Table 1). The quality of the structure can be assessed from the electron density map (Figure 2b), from the Ramachandran plot (91.5% of the residues are located in the most favorable areas (20)), and from the R - and free R -factors (21% and 28%, respectively). The C α atoms of the β -barrels of the RR6–VHH were superimposed on the C α atoms of the hCG–VHH (7) and Lys–VHH (5), giving a very low rms deviation of 0.58 \AA for both molecules. The nature of the molecular surfaces of the three VHHs is also comparable, each presenting a highly hydrophilic surface on the side of the VHH normally packed against the VL in a classical Fv fragment (5–7 and the present result).

The VHH CDR Loops. The three CDR loops are well-defined in density (Figure 3). The CDR1 loop, being the most exposed to solvent, exhibit B -factors higher than average, as often observed in classical antibodies (28.5 \AA^2 compared to 24.6 \AA^2). The CDR2 and the long CDR3 loops, however, display B -values lower than average (17 and 16 \AA^2 , respectively, compared to 24.6 \AA^2). Canonical conformations have been assigned to five of the six CDR loops of IgGs (21–23). Comparison of VHH CDR loops with loops of canonical type showed that camel H1 loops, in Lys–VHH and RNase–VHH, have identical, non previously identified canonical conformations (5–6). They have been attributed to a new canonical type (type 4, ref 6). The H1 loop of the hCG–VHH (7) has no identified canonical type and the H1 loop of the RR6–VHH complex also has a different, noncanonical, conformation. The sequence of the latter is three residues longer than those of the VHHs mentioned above, with the insertion of a His-Gly-His motif (Figure 1). The further comparison of VHH CDR loops with canonical types showed that the H2 CDRs of both hCG–VHH and Lys–VHH belong to canonical type 2, although type 3 has been predicted from the sequence of Lys–VHH. In contrast, the RNase–VHH H2 loop was not found to belong to any

	110	120	301	abc	140	501	abc	601
LAMA-RR6	QVQLQESGGGLVQAGGSLRLS	CAASGRAT	SGHGH	YGMGWFRQVPGKEREFV	AAIRW	--	SGKETWYKDSV	
LAMA-hCG	QVQLQESGGGLVQAGGSLRLS	CAASGRT	TGST	---YDMGWFRQAPGKERESV	AAINW	--	DSARTYYASSV	
CAMEL-Lys	DVQLQASGGGSVQAGGSLRLS	CAASGYT	IGP	---YCMGWFRQAPGKEREGV	AAINM	--	GGGITYYADSV	
CAMEL-RNase	QVQLVESGGGLVQAGGSLRLS	CAASGYA	ITY	---IYMGWFRQAPGKEREGV	AAMDS	--	GGGGTLYADSV	
	701	801	abc	901	1001	abcdefghijklmno		1110
LAMA-RR6	KGRFTISRDNAKTTVYLQMN	SLKPEDTAVYY	CAARPVRVDDISLPVGF	-----		DYWGQGTQVTVSS		
LAMA-hCG	KGRFTISRDNAKTTVYLQMN	SLKPEDTAVYT	CGAGEGGTW	-----		DSWGQGTQVTVSS		
CAMEL-Lys	KGRFTISQDNAKNTVYLLMNS	LEPEDTAIYY	CAADSTIYASYECGHLSTGGYGYDSWGQGTQVTVSS					
CAMEL-RNase	KGRFTISRDKGKNTVYLQMD	SLKPEDTATYY	CAAGGYELDRDY	-----		GQWGQGTQVTVSS		

FIGURE 1: Amino acid sequences of the four VHH fragments of known structure: the anti-RR6(R2)–VHH (this work), the llama hCG–VHH (7), the camel Lys–VHH (5), and the RNase–VHH (6). The three CDRs (1 to 3) are in bold letters. The numbering is according to Kabat (31).

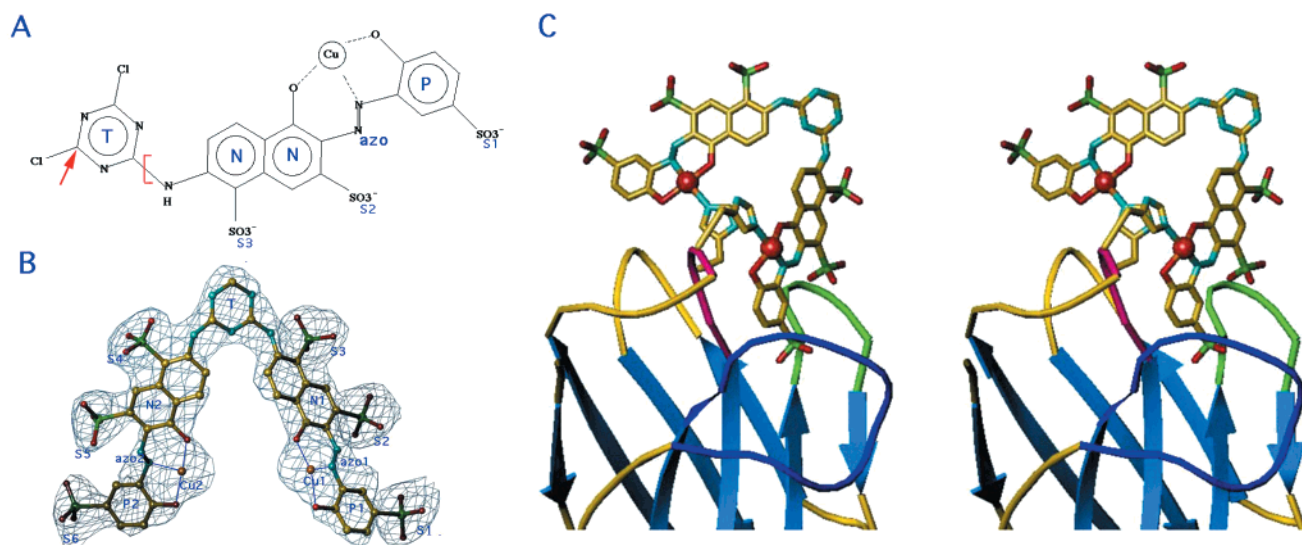


FIGURE 2: Structure of the RR6 hapten in complex with the llama VHH (a) The chemical formula of the RR6 molecule. The sulfate groups have been numbered S1–S3. P stands for p-sulfonyl-phenol, N for naphthyl moiety, and T for triazine. The red arrow indicates the insertion site of another P+N fragment (as indicated by the bracket) on a second reactive position of the triazine ring. (b) The RR6 molecule and its electron density map contoured at 1 sigma threshold. No atom is visible at the third position of the triazine ring in the electron density map. (c) Stereoview of the RR6 molecule in complex with the VHH fragment. The top half of the VHH fragment is displayed in secondary structure representation with the β -strands in blue, the loops in yellow, and the CDRs 1, 2, 3 in red, green, and blue, respectively. The RR6 molecule is in ball-and-stick representation, with the copper ions as red spheres complexed with the side-chain of histidines 31a (right) and 31c (left).

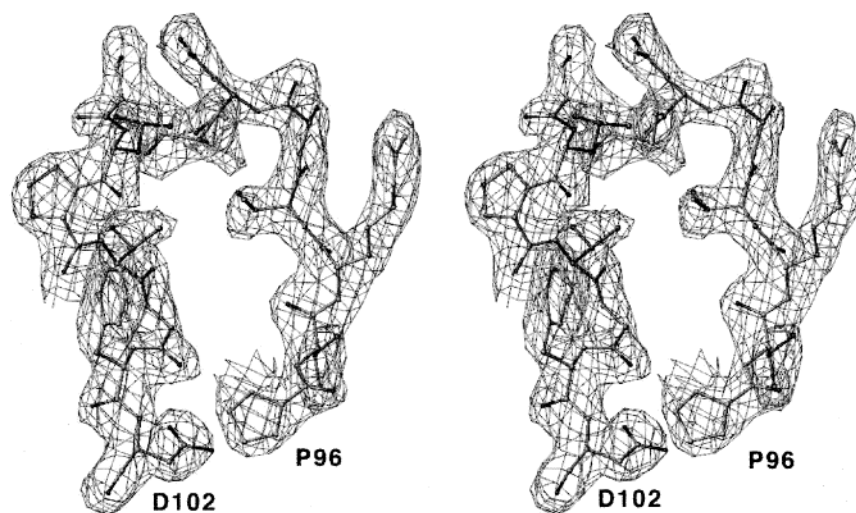


FIGURE 3: Stereoview of the electron density map (2Fo–Fc contoured at 1s) of the VHH CDR3 between Pro96 and Asp102.

identified canonical type (6). In the present structure, the conformation of loop H2 belongs to canonical type 3.

Camelid VHH sequences indicate that H3 loops are generally longer than murine or human loops (2, 3, 4). This

was the case for the Lys–VHH fragment, with a very long H3 loop of 24 residues held together by an internal disulfide bridge (5). In contrast, the RNase–VHH (6) CDR3 is only 12 residues long and the hCG–VHH H3 loop is reduced to

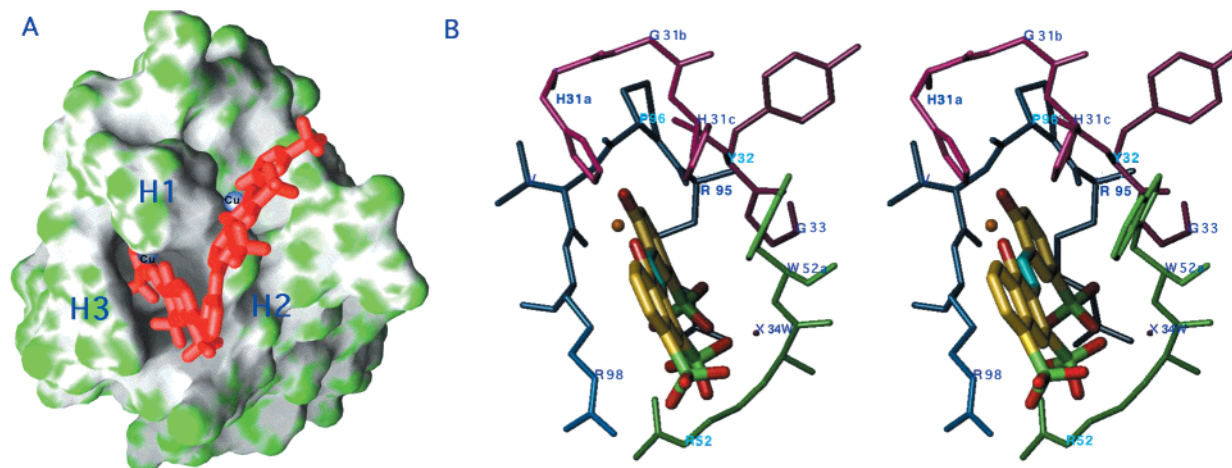


FIGURE 4: The combining site of the anti-RR6-VHH and the RR6 inside, viewed from the top. (a) Water-accessible surface of the VHH displaying the cavities, with the bound RR6 molecule (red) in ball-and-stick representation, with the copper ions as silvery blue spheres. The green color identifies the protruding surfaces, and the gray color identifies the reentering surfaces (GRASP representation, 32). The localization of the three CDRs has been indicated by H1, H2, and H3. (b) Stereoview of the P1 and N1 groups of the P1+N1 groups of the RR6 molecule in complex with the 3 CDRs of the anti-RR6-VHH fragment. The CDRs 1–3 are red, green, and blue, respectively.

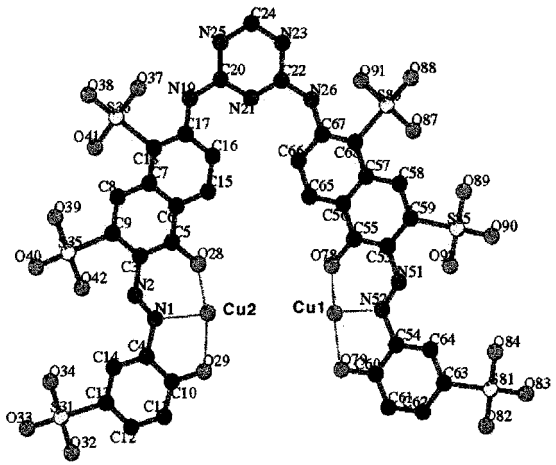
a mere eight residues long stretch (7). The two latter CDR3 are, therefore, within the length range observed in H3 loops of normal VH domains (Figure 1) (4). The anti-RR6-VHH CDR3, with 14 residues, is comparable in length to that of the RNase-VHH (6). It might, therefore, be expected to play a substantial role in the interaction with the hapten. This is not the case, however (see below).

The Azo-dye RR6 Hapten. The electron density maps and the copper ion anomalous signal indicated the presence of two copper ions per VHH fragment. This was confirmed by the structure solution and refinement. This unexpected stoichiometry was attributed to a chemical modification of the RR6 hapten, resulting in the fusion of a second P + N motif at a second reactive position of the triazine ring (Figure 2, a and b). Mass spectroscopy, performed with the original RR6 hapten, indicates that the RR6 monomer (the non-duplicated form) is by far (>95%) the predominant form, the rest being represented by copper-depleted fragments and the dimer. Considering that the molar ratio RR6-VHH in the crystallization conditions is only 5, the amount of RR6 dimer initially available for complexation with the VHH is very low. Therefore, duplication should have occurred during the crystal growth. Another strong argument for the duplication during crystallization is the fact that the RR6 hapten has to be coupled to BSA in order to be immunogenic. This coupling is performed using the reactive triazine ring. The almost complete lack of reactivity of the third position of the triazine ring once the two first positions have been substituted (the case of the RR6 dimer) prevents any coupling of a putative preexisting RR6 dimer to BSA. Therefore, the RR6 dimer cannot be the “authentic” hapten used for immunization. Accordingly, the dissociation constant, which is measured on the monomer, is probably slightly lower compared to that of the dimeric RR6 hapten.

The Combining Site. Two cavities are present at the surface of the VHH combining site, one of which is occupied by the tip of the hapten, and the other is empty (Figure 4a). The hapten molecule has 41% of its surface buried in the VHH, the rest of it, in particular, the triazine ring and the second part of the dimer, are exposed to the solvent. A high-solvent exposure of the triazine group was expected, because

during immunization this group was coupled to BSA and, therefore, not freely accessible. The surface complementarity between the VHH and the hapten is excellent, as indicated by the large interaction surface area of the CDRs with the RR6: CDR1 residues 31a–33 have an interaction surface of 127 Å², the majority of which (104 Å²) arises from the RR6 copper atoms interacting with the two histidines. CDR2 interacts with residues 52–53 to an amount of 99 Å². Among the three CDRs, the long CDR3 provides the smallest interacting surface area, 69 Å², with residues 95–98 (Figures 2c and 4b), in striking contrast with the structure of Lys-VHH and other results with classical antibodies. Most of the CDR3 loop is turned outward from the β -barrel (Figure 2c). Overall, the RR6 hapten covers 295 Å² of the VHHs accessible surface. The first half of the RR6 dimer, corresponding to the authentic (P + N + T), has 60% of its surface buried in the VHH. Its P1 group and two sulfate groups (S1 and S2) are embedded between the three CDRs, and His31a (from CDR1) is linked to the copper belonging to the N1 moiety. A second histidine (His 31c) from the CDR1 is linked to the other copper and is the only contact of the second half of the RR6 dimer with the VHH. This result further confirms the monomer as being the authentic hapten. The N ϵ 2 of these histidines complete the ligation of the copper ions in a distorted square-planar conformation (Figures 2c and 4). The interaction of the both histidine residues with the copper ion belonging to the first part of the RR6 has been modeled. A simple side-chain rotation is sufficient to bring the N ϵ 2 atom in a favorable position and complete the square-planar coordination in an axial fashion. This type II copper coordination has been observed in several copper proteins such as superoxide dismutase, oxygenases, nitrite reductase, and various oxidases (see <http://bmbsgi11.leeds.ac.uk/bmbknd/promise/html>).

The Binding Forces Involved in Interaction. Two main driving forces have been found to account for antigen binding: the hydrophobic effect (liberation of water molecules from apolar protein surfaces upon complex formation) and enthalpic forces (24). The contribution of each of the two forces to complex formation differ greatly in antibodies, even directed to the same target (25). In general, the

Table 2: List of the Main Contacts Between the RR6-Dye Dimer and the VHH^a


31a	HIS	Nε2	CU1	2.20
31c	HIS	Nε2	CU2	2.32
52	ARG	Nη1	O82	3.15 H-bond
52a	TRP	N	O92	3.24 H-bond
53	SER	N	O92	2.93 H-bond
53	SER	Oγ	O89	2.84 H-bond
53	SER	Oγ	O92	2.94 H-bond
55	LYS	NZ	O87	2.75 H-bond
55	LYS	NZ	O91	2.97 H-bond
95	ARG	Cδ	O83	3.46
96	PRO	O	C61	3.35
97	VAL	C	C62	3.44
98	ARG	Cα	C62	3.50
98	ARG	Cγ	C64	3.48
98	ARG	Nε	O90	2.90 H-bond
99	VAL	N	O82	3.14 H-bond
34W	WAT	OW	O83	2.81 H-bond

^a Cutoff is 3.7 Å, but only one atom has been kept per residue (except for H-bonds). The RR6 numbering is indicated below (the most buried part of the RR6 hapten is on the right side).

specificity of antibodies is dependent on the nature of the binding surface and on the formation of charge–charge interactions and hydrogen bonds, an example being steroid hormones (26–28). There are, however, examples of specific binding arising solely from shape complementarity in the absence of any electrostatic interaction (29).

In the VHH–RR6 complex, hydrophobic forces are present but hydrogen bonds and charge interactions dominate (Table 2). The naphthyl moiety is in stacking contact with Trp52A and the charged S1 group interacts through a dense network of hydrogen bonds with the side chains of Arg52, and with main-chain atoms, NH52a and NH99. Water molecule 34w closes the bottom of the site, interacting with the hapten S1 on one side and with Arg95 Nη1 and Ile51 CO group on the other. The P1 ring is in van der Waals contact with most atoms of the combining site. Besides this first moiety, the sulfate S2, located on the naphthol group N1, is hydrogen bonded to Arg98 Nε, to Ser53 Oγ, and NH atoms. Apart from the copper–histidine binding, no other contacts occur between the VHH and the hapten beyond S2 (Table 2, Figure 4).

CONCLUDING REMARKS

The RR6 dimer is a very large hapten, which possesses an unusual combination of chemical moieties: several

aromatic rings, two copper ions, and numerous charged groups. The anti-RR6–VHH was found to provide a good combining site to the RR6 hapten using its three CDRs. Despite the absence of a VL, this site forms a deep cleft, which involves only residues from the CDRs and none from the framework. Both hydrophobic and electrostatic effects are likely to be important for establishing the binding. Finally, ability of a camelid VHH to bind to a copper ion also suggests the valuable possibility of using these fragments as redox proteins, which would disclose new lines of approach in abzyme research (30).

ACKNOWLEDGMENT

The ESRF is greatly acknowledged for beam time allocation at BM14. We would like to thank Gordon Leonard for helping during data collection (BM14, ESRF). Sabine Diotallevi, Philippe Cantau, and the UNILEVER research group are greatly acknowledged for technical assistance.

REFERENCES

- Hamers-Casterman, C., Atarhouch, T., Muyldermans, S., Robinson, G., Hamers, C., Songa, E. B., Bendahman, N., Hamers, R. (1993) *Nature* 363, 446–448.
- Ghahroudi, M. A., Desmyter, A., Wyns, L., Hamers, R., and Muyldermans, S. (1997) *FEBS Lett.* 414, 521–526.
- Frenken, L., Hamers, R., Hamers-Casterman, C., Muyldermans, S., and Verrips, T. (1994) Production of antibodies or (functionalized) fragments thereof derived from heavy chain immunoglobulins of CAMELIDAE., patent number WO 94/25591.
- Vu, K. B., Ghahroudi, M. A., Wyns, L., and Muyldermans, S. (1997) *Mol. Immunol.* 34, 1121–1131.
- Desmyter, A., Transue, T. R., Ghahroudi, M. A., Thi, M. H., Poortmans, F., Hamers, R., Muyldermans, S., Wyns, L. (1996) *Nature Struct. Biol.* 3, 803–811.
- Decanniere, K., Desmyter, A., Lauwereys, M., Ghahroudi, M. A., Muyldermans, S., Wyns, L. (1999) *Structure* 7, 361–370.
- Spinelli, S., Frenken, L., Bourgeois, D., de Ron, L., Bos, W., Verrips, T., Anguille, C., Cambillau, C., and Tegoni, M. (1996) *Nature Struct. Biol.* 3, 752–756.
- Transue, T. R., De Genst, E., Ghahroudi, M. A., Wyns, L., and Muyldermans, S. (1998) *Proteins* 32, 515–522.
- Lauwereys, M., Arbabi Ghahroudi, M., Desmyter, A., Kinne, J., Holzer, W., De Genst, E., Wyns, L., Muyldermans, S. (1998) *EMBO J.* 17, 3512–3520.
- Alzari, P. M., Spinelli, S., Mariuzza, R. A., Boulot, G., Poljak, R. J., Jarvis, J. M., and Milstein, C. (1990) *EMBO J.* 9, 3807–3814.
- Wilson, I. A., and Stanfield, R. L. (1994) *Curr. Opin. Struct. Biol.* 4, 857–867.
- Leon, G. J., Frenken, R. H. J., van der Linden, Pim W. J. J. Hermans, J. Wil Bos, Robin C. Ruuls, Bernard de Geus, and C. Theo Verrips. Isolation of antigen specific Llama V_HH antibody fragments and their high level secretion by *Saccharomyces cerevisiae*. *J. Biotech.*, in press.
- Otwinowski, Z., Minor, W. (1997) *Methods Enzymol.* 276, 307.
- Collaborative Computational Project, No.4. (1994) *Acta Crystallogr. D* 50, 760.
- Sheldrick, G. M. (1990) *Acta Crystallogr. A* 46, 467.
- Navaza, J. (1994) *Acta Crystallogr. A* 50, 157.
- Roussel, A., Cambillau, C. (1989) in *Silicon Graphics Geometry partner directory (Fall 1989)* (Silicon Graphics, Ed.) pp 77–78. Mountain View, California.
- Brunger, A. T., Kuriyan, J., Karplus, M. (1987) *Science* 35, 458.
- Brunger, A. T. (1996) XPLOR version 3.843 Manual. New Haven, Connecticut: Yale University Press.
- Laskowski, R., MacArthur, M., Moss, D., and Thornton, J. (1993) *J. Appl. Crystallogr.* 26, 91.

21. Chothia, C., Lesk, A. M., Tramontano, A., Levitt, M., Smith-Gill, S. J., Air, G., Sheriff, S., Padlan, E. A., Davies, D., Tulip, W. R., Colman, P. M., Spinelli, S., Alzari, P. M., and Poljak, R. (1989) *Nature* 342, 877–883.
22. Martin, A. C., Thornton, J. M. (1996) *J. Mol. Biol.* 263, 800–815.
23. Al-Lazikani, B., Lesk, A. M., Chothia, C. (1997) *J. Mol. Biol.* 273, 927–948.
24. Mariuzza, R. A., Poljak, R. J., and Schwarz, F. P. (1994) *Res. Immunol.* 145, 70–72.
25. Malby, R. L., Tulip, W. R., Harley, V. R., KcKimm-Breschkin, J. L., Laver, W. G., Webster, R. G., and Colman, P. M. (1994) *Structure* 2, 733.
26. Webster, D. M., Henry, A. H., and Rees, A. R. (1994) *Curr. Opin. Struct. Biol.* 4, 123.
27. Trinh, C. H., Hemmington, S. D., Verhoeyen, M. E., and Phillips, S. E. V. (1997) *Structure* 5, 937.
28. Arevalo, J. H., Stura, E. A., Taussig, M. J., and Wilson, I. A. (1993) *J. Mol. Biol.* 231, 103.
29. Jeffrey, P. D., Strong, R. K., Sieker, L. C., Chang, C. Y., Campbell, R. L., Petsko, G. A., Haber, E., Margolies, M. N., Sheriff, S. (1993) *Proc. Natl. Acad. Sci. U.S.A.* 90, 10310–10314.
30. Quilez, R., de Lauzon, S., Desfosses, B., Mansuy, D., and Mahy, J. P. (1996) *FEBS Lett* 395, 73.
31. Kabat, E. A., Wu, T. T., Perry, H. M., Gottesman, K. S., Foeller, C. (1991) ed. 5, Bethesda, National Institute of Health.
32. Nichols, A. (1991) *Proteins: Struct. Funct. Genet.* 11, 281.

BI991830W